Supplementary Information

350 ps Ultrafast Room-Temperature Scintillation Realized on $CsPbBr_3$-Based Single Crystals via Br_2 Over-Doping

Zongxiao Li,[a,b,c] Xiaoping Ouyang,[d] Zhifang Chai,[a,c] Duck Young Chung,[e] Fangbao Wang,[d] Yihui He,[h] Tao Bo,[a,c] Wenwen Lin, [*a,c,e,f] and Mercouri G. Kanatzidis[*e,f,g]

[a]Zhejiang Key Laboratory of Data-Driven High-Safety Energy Materials and Applications, Ningbo Key Laboratory of Special Energy Materials and Chemistry, Laboratory of Advanced Nuclear Materials, Ningbo Institute of Materials Technology and Engineering (NIMTE), Chinese Academy of Sciences, Ningbo 315201, China

[b]University of Chinese Academy of Sciences, Beijing, 100049, China

[c]Qianwan Institute of NIMTE, Ningbo 315336, China

[d]State Key Laboratory of Intense Pulsed Radiation Simulation and Effect and Radiation Detection Research Center, Northwest Institute of Nuclear Technology, Xi'an 710024, China

[e]Materials Science Division, Argonne National Laboratory, Lemont, Illinois 60439, United States

[f]Department of Chemistry, Northwestern University, Evanston, Illinois 60208, United States

[g]Department of Materials Science and Engineering, Northwestern University, Evanston, IL, 60208 USA

[h]State Key Laboratory of Radiation Medicine and Protection, Collaborative Innovation Center of Radiological Medicine of Jiangsu Higher Education Institutions, and School for Radiological and Interdisciplinary Sciences (RAD-X), Soochow University, Suzhou, China

Experimental section

Materials

Chemicals were used as obtained: $PbBr_2$(99.999% purity, Aladdin),CsBr (99.999% purity, Aladdin), liquid bromine (99.5% purity, Hushi).

The synthesis of cesium tribromide powder was carried out within a fume hood. Cesium bromide powder (2.1281 g, 0.01 mol) and an excessive amount of liquid bromine (approximately 1.8 g, 0.01126 mol) were introduced into a round-bottom flask. Subsequently, the flask was immersed in an oil bath maintained at 80 °C for 1 hour. This was done to guarantee the complete reaction between cesium bromide and bromine, thereby yielding cesium tribromide. Once all of the excessive liquid bromine had fully evaporated, the residual orange end product at the bottom of the flask was carefully collected. The powder X-ray diffraction (PXRD) pattern of the orange substance authenticated it as a pure phase cesium tribromide, as presented in Fig. S1.

Crystal growth and methods

(1) Initially, the quartz tube was immersed in a hydrofluoric acid (HF) solution with a concentration of 2% for 6 hours. Subsequently, the inner wall of the quartz tube was rinsed with deionized water and anhydrous ethanol no less than three times. Finally, it was dried in an oven at 120 ℃ for 10 hours.

(2) First, the precursors (0.3354 g of $CsBr_3$ (0.00090 mol), 22.0206 g of $PbBr_2$ (0.0600 mol), 12.5771 g of CsBr (0.0591 mol)) were loaded into a quartz tube with an inner diameter of 12 mm and an outer diameter of 14 mm. Subsequently, the quartz tube was evacuated and sealed under a residual pressure of approximately 4E-3 mbar.

(3) The precursors were pre-synthesized into $CsPbBr_{3.03}$ polycrystalline ingots at 700 ℃ using a rocking furnace before processing. Then the quartz tube was mounted within the top high-temperature zone of the Bridgman furnace. The three furnace zones were heated to their respective target temperatures (540-580-420 ℃) with a ramp time of 6-8 h. Such a setting enabled the temperature gradient in the crystallization region (near 537.5 ℃) to be 6.7 ℃/cm.

Crystal processing and characterization

The grown crystal ingots were cut into wafers with a thickness of 1.35 mm, with an infeed speed of 0.5 mm/min. Wafers were mechanically polished through subsequently finer grits (1500, 3000, 5000 and 7000 mesh SiC sand papers), and then the surface was further polished using a 0.5-micron diamond polishing suspension to achieve an ultra-smooth surface. The polished wafer (approximately 0.8 mm in thickness) is shown in Fig.1 (e), demonstrating enhanced transmittance.

Powder X-ray diffraction (PXRD) measurement and refinement

The powder X-ray diffraction (PXRD) analysis was performed using a Bruker D8 Advance instrument equipped with a Cu *K*α radiation source (*λ*= 1.5406 Å), operated at a voltage of 40 kV and a current of 40 mA. The 2 theta ranges from 5° to 90° with an angle step of 0.02°. The obtained PXRD patterns were indexed using a simulated pattern to identify the types of phases and phase purity. Following this, the Rietveld refinement of the powder X-ray diffraction data was carried out using Bruker's TOPAS software.[1] This method calculates the powder diffraction pattern by employing a specific peak shape function that is based on the initial crystal structure model and the input parameters. The crystal structure and peak-shape parameters are continuously adjusted via the least-squares method. This enables the calculated diffraction pattern to match the experimental one, thus yielding accurate structural parameters.

Resistivity Test

The wafer was processed into dimensions of 5.0×5.0 mm^2 with a thickness of 1.0 mm, followed by current-voltage (*I*-*V*) characterization.

The magnetron sputtering method was employed to deposit gold electrodes on the top and bottom surfaces of the wafer. The coating current for magnetron sputtering was set at 30 mA, and the deposition time was 300 s. Subsequently, copper tapes were attached to both opposite edges of the quartz plate as an insulating substrate. A copper wire with a diameter of 0.1 mm was used to connect the copper tapes to the gold electrodes on the wafer. The connection points were secured with silver paint,

and meanwhile, the wafer was fixed onto the quartz plate. The fabricated device was placed in a sealed box. The Al box serves to provide electromagnetic shielding and a light-free environment. The dark current of the device and the resistivity of the material are evaluated by means of the Keithley 6517B source meter.

Thermal analysis

The thermal properties of $CsPbBr_3$ and $CsPbBr_{3.03}$ samples were analyzed using a Shimadzu DTA-50 thermal analyzer. A small amount of sample (～40 mg) was sealed in a tiny quartz bottle. The samples were heated to 550 °C at a rate of 2.0 °C·min^{-1}, held at this temperature for 6 h, and then cooled to 70 °C at a rate of 5.0 °C·min^{-1}. Subsequently, a second cycle was carried out under the same experimental conditions to verify the repeatability of the result. The melting point and solidification temperature of the samples were determined at the minimum of the endothermic peak and the maximum of the exothermic peak, respectively.

The measurements of the band gap

The Hitachi UH-4150 spectrophotometer was used to measure the optical diffuse reflection in the 200-2500 nm wavelength range to determine the band gap at room temperature. Barium sulfate was selected as the reference baseline. The sample was ground into powder and compacted. The Tauc plot method was used to determine the band gap, with *n* taking 1/2. A polished wafer with a thickness of 1.5 mm was selected to test the transmission spectrum on a PerkinElmer Lambda 1050+. The data acquisition wavelength range was 400-800 nm, with an interval of 1 nm.

Measurement of photoluminescence spectroscopy

Emission spectroscopy and time-resolved photoluminescence (PL) measurements on cleavage surfaces were carried out using an Edinburgh FSL1000 spectrometer. In order to avoid the disturbance of surface states and distortion of lattice after polishing on PL spectra, cleaved $CsPbBr_3$ and $CsPbBr_{3.03}$ chunks without polishing were extracted for PL tests. The Edinburgh FLS1000 photoluminescence spectrometer was equipped with a 375 nm laser source with a power of 5 mW, a time-correlated single photon counting (TCSPC) module for lifetime measurements, and a PMT-900 photomultiplier

tube detector. The cleaved $CsPbBr_3$ and $CsPbBr_{3.03}$ chunks were mounted into the sample holder module. The PL of the sample was excited with a 375 nm laser (5 mW). The laser source hit the sample at 45° with a distance of around 10 cm. The emission slit width for detection was set to 5 nm. The PL data were collected from the emission range of 400 to 800 nm with a 1.0 nm interval and a 0.5 s dwell time. We also employed the instrument to perform temperature-dependent photoluminescence measurements on the sliced samples. The samples were mounted on a vertical holder and cooled to 80 K using liquid nitrogen. A 375 nm (5 mW) laser was utilized to excite the samples in the wavelength range of 400-700 nm. A 400 nm long-pass filter was placed along the receiving end path. The acquired TRPL data is analyzed using the FAST module integrated within the software. This allows for the determination of the decay time of each component in the sample.

Measurement of radioluminescence spectra

At room temperature, radioluminescence spectra measurements were carried out for freshly cleaved surfaces of the $CsPbBr_3$ and $CsPbBr_{3.03}$ samples using an Edinburgh FSL1000 fluorescence spectrometer. The receiving end comprises a time-correlated single-photon counting (TCSPC) module used for lifetime measurement and a photomultiplier tube (PMT-980) detector. The samples were irradiated with 5.31 MeV α particles from a ^{210}Po isotope source. The source had an activity of 5.0 mCi (185 MBq). The radiation source was positioned facing the sample and irradiated it at a 45-degree angle, maintaining a distance of approximately 1 cm. The width of the detection emission slit was set to 0.5 nm. For the RL data acquisition, the wavelength range spanned from 400 to 800 nm, with a 1 nm interval and a 0.5 s dwell time.

X-ray-induced radioluminescence and imaging

The temperature-dependent X-ray radioluminescence spectral analysis of the cleavage planes of $CsPbBr_{3.03}$ and $CsPbBr_3$ samples was carried out using the Zolix FLS-XrayV series fluorescence spectrometer. The excitation light was filtered using a 400-nm long-pass filter. The photon signals were collected by the PMT at the end of the wavelength range of 400 - 800 nm. The X-rays were generated using the OmniFluo960-

XrayP-Z system from Zolix, which is equipped with a tungsten-target X-ray tube with a maximum power of 50 W. The output X-ray dose can be adjusted by varying the operating tube current and voltage. The dosage of X-rays was calibrated by Ningbo Institute of Metrology and Testing Research. For the X-ray imaging test, the pattern used is a TYPE39b line-pair card. It has a thickness of 0.03 mm and a maximum resolution of 30 line pairs per millimeter.

Measurement of single photon time spectra

The luminescence decay curves of α particles were measured using the dual-channel single photon correlation (DCSPC) method. In this method, a photomultiplier tube (Hamamatsu, R7899) was employed to record a specific scintillation event, while a micro-channel plate (Hamamatsu R3809U-52) was utilized to detect single photons randomly emitted during the scintillation event. The scintillator was mounted on a photomultiplier tube (Hamamatsu, CR173-Q1) to acquire the pulse height spectrum. The amplified signals were analyzed using a multichannel analyzer (ORTEC ASPEC-927). A PMT (ET Enterprises, 9815B) was coupled to an oscilloscope (Teledyne LeCroy, HDO8108A) for the collection of single particle waveforms. During the testing process, the sample was directly positioned on the receiving window of the PMT. The $CsPbBr_{3.03}$ sample, the PMT, and the isotope source were placed within a light-tight box. α particles were sourced from ^{241}Am isotope sources. The crystal sample was placed adjacent to the receiving window of the photomultiplier tube. The radioactive source (^{241}Am isotope) was fixed on a platform and located in close proximity to the crystal. All of the aforementioned components were housed within a light-tight enclosure to mitigate the influence of ambient light. The high voltage was supplied by a DC high voltage source. The signals from the photomultiplier tube were recorded using an oscilloscope with a sampling rate of 10 GHz. For each sample and radioactive source combination, over 1000 waveforms were recorded.

Scanning Electron Microscope - Energy Dispersive Spectrometer (SEM-EDS)

The morphology observation, Energy Dispersive Spectroscopy (EDS) analysis, and elemental mapping measurements of the samples were performed using a Zeiss Sigma

300 thermal field emission scanning electron microscope. The accelerating voltage was set to 15 kV. The proportion of bromine in the as-grown crystals was identified and qualitatively assessed via EDS analysis.

X-ray photoelectron spectroscopy (XPS)

X-ray Photoelectron Spectroscopy (XPS) measurements were performed using a Shimadzu AXIS SUPRA+ spectrometer to characterize the elemental composition and chemical states of the material surface.

Scanning Probe Microscopy (SPM)

SPM was employed to investigate the surface of materials at the nanoscale, primarily for characterizing surface topography. The measurements utilized an intelligent scanning mode with a scanning range of 5 μm × 5 μm (in the xy-plane).

Computational method

All density functional theory (DFT) calculations in this work were performed using the Vienna Ab-Initio Simulation Package (VASP).[2] The electron-ion interaction was described by the projector augmented wave (PAW) method,[3] and the Perdew-burke-Ernzerh of generalized gradient approximation (PBE-GGA)[4] exchange-correlation functional was employed. All calculations were performed using a plane-wave cutoff energy of 550 eV and Gaussian smearing with a width of σ = 0.10 eV. The 2×2×2 and 2√2×2√2×2 supercell models of $CsPbBr_3$ were used to calculate the doping of a single Br atom and Br_2 molecule, respectively. Brillouin zone integration was carried out using a Monkhorst-Pack k-point mesh of (1 × 1 × 1)[5]. The self-consistent field (SCF) iterations were considered converged when the energy change fell below 1×10^{-5} eV, and atomic positions were fully relaxed until the maximum force on any atom was less than 0.005 eV $Å^{-1}$. The formation energy of interstitial Br atoms (E_f) is calculated according to the following formula:

$$E_f = (E_{crystal+Br} - E_{crystal} - n_{Br}E_{Br})/n_{Br},$$

where $E_{crystal+Br}$ represents the energy of $CsPbBr_3$ after Br doping, $E_{crystal}$ indicates the energy of $CsPbBr_3$, E_{Br} represents the energy per atom for a Br_2 molecule, and n_{Br} represents the number of Br atoms incorporated into the crystal.

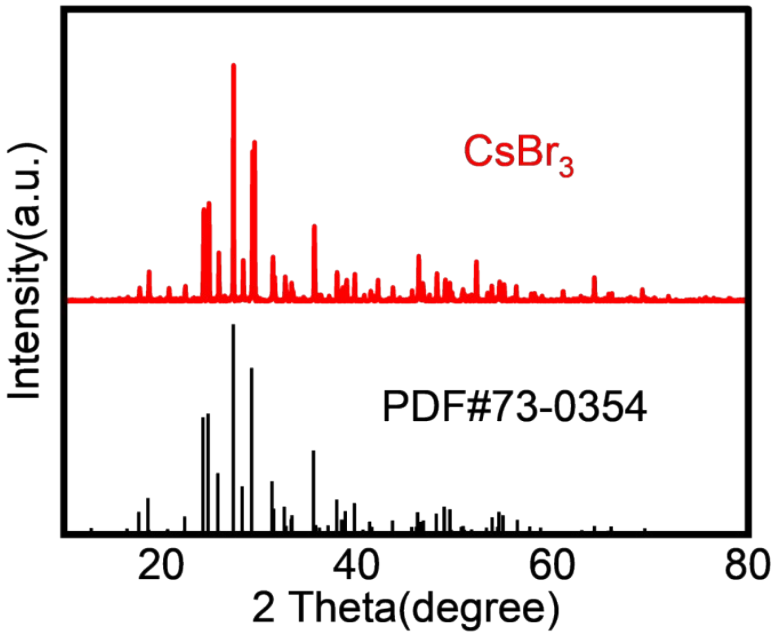

Fig. S1 PXRD pattern of as-synthesized $CsBr_3$.

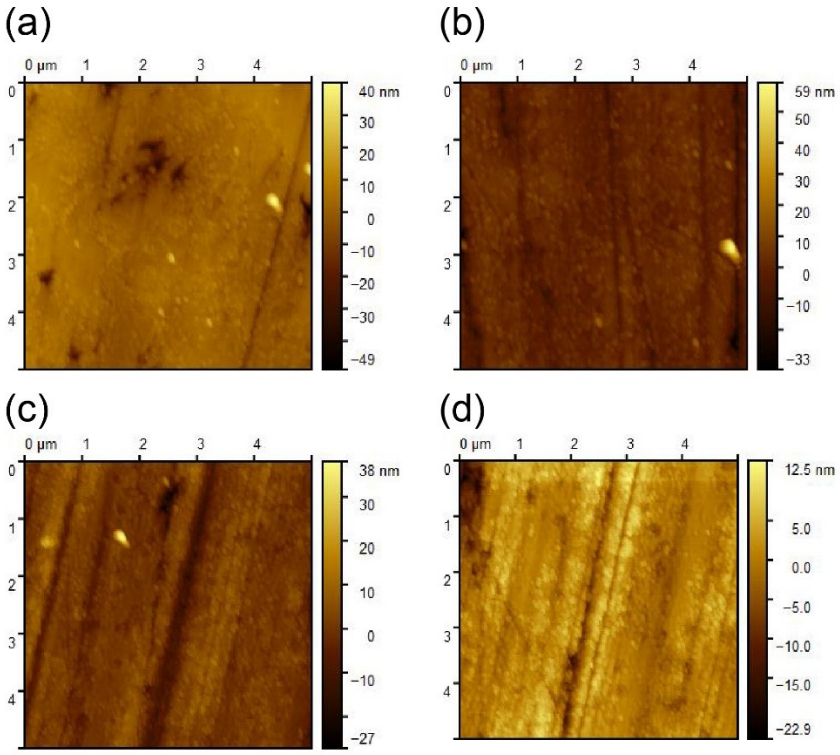

Fig. S2 (a)-(b) Atomic Force Microscope (AFM) micrographs of the surface of $CsPbBr_3$ single crystals measured in air. (c)-(d) AFM micrographs of the surface of $CsPbBr_{3.03}$ single crystals measured in air.

Table S1. Room temperature lattice constants of the undoped $CsPbBr_3$ powders and the over-doped $CsPbBr_{3.03}$ powders (for simplicity, the data were refined using the orthorhombic model Pnma).

Samples	$CsPbBr_3$	$CsPbBr_{3.03}$	Expansion
a (Å)	8.25470±0.00070	8.26078±0.00458	0.0737%
b (Å)	8.20215±0.00064	8.22105±0.00364	0.2304%
c (Å)	11.75455±0.00087	11.76773±0.00541	0.1121%
V (Å^3)	795.856684±0.108973	799.173296±0.675675	0.4167%
α (°)	90	90	
β (°)	90	90	
γ (°)	90	90	

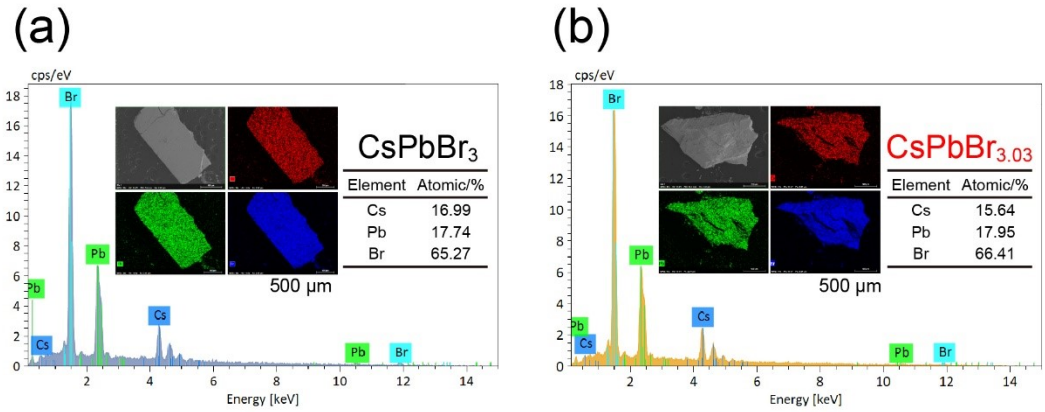

Fig. S3 (a) SEM-EDS testing of the $CsPbBr_3$ single crystal. (b) SEM-EDS testing of the $CsPbBr_{3.03}$ single crystal.

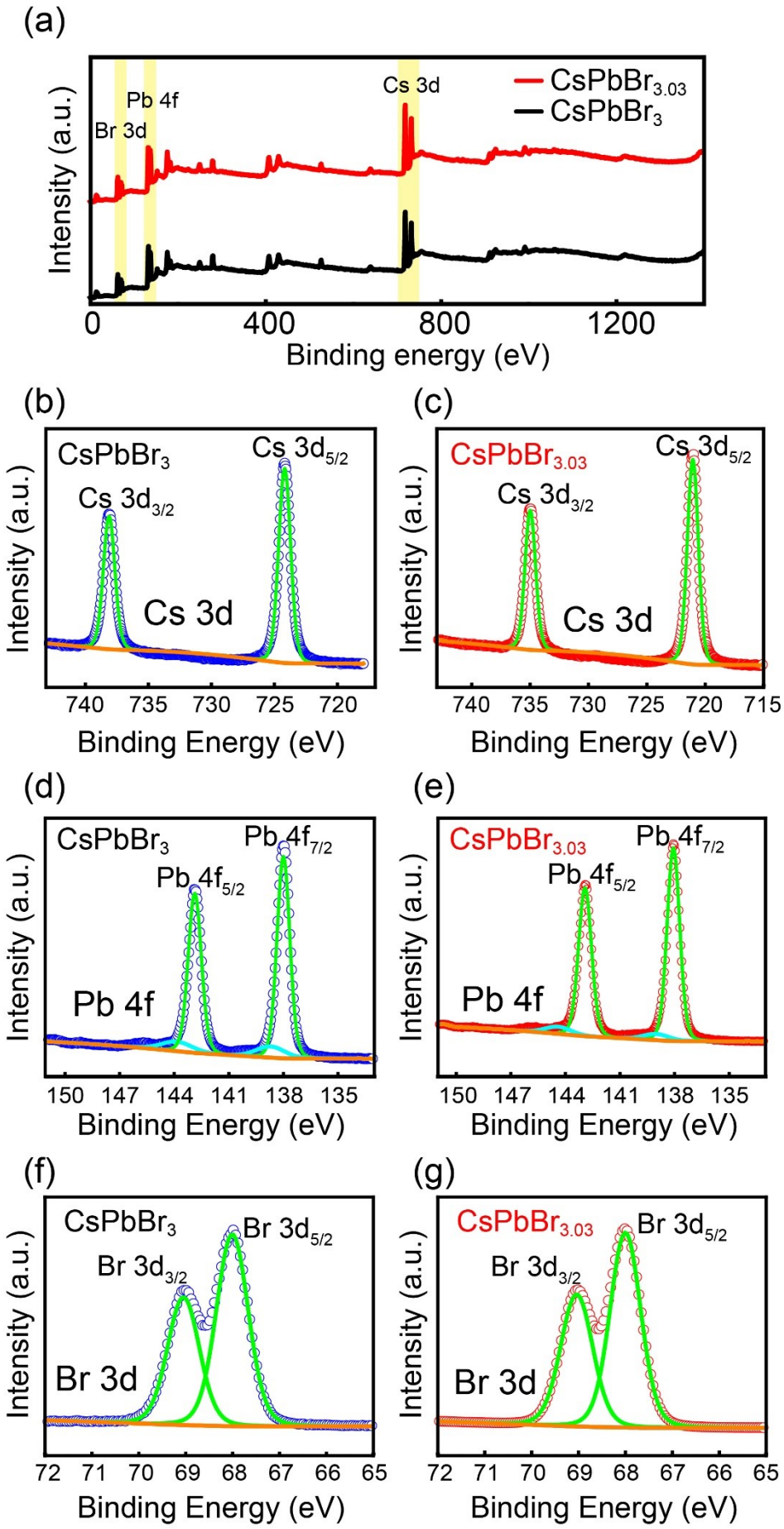
(a)
Intensity (a.u.)
Pb 4f
Br 3d
Cs 3d
CsPbBr3.03
CsPbBr3
0
400
800
1200
Binding energy (eV)
(b)
CsPbBr3
Cs 3d5/2
Cs 3d3/2
Cs 3d
Intensity (a.u.)
740 735 730 725 720
Binding Energy (eV)
(c)
CsPbBr3.03
Cs 3d5/2
Cs 3d3/2
Cs 3d
Intensity (a.u.)
740 735 730 725 720 715
Binding Energy (eV)
(d)
CsPbBr3
Pb 4f7/2
Pb 4f5/2
Pb 4f
Intensity (a.u.)
150 147 144 141 138 135
Binding Energy (eV)
(e)
CsPbBr3.03
Pb 4f7/2
Pb 4f5/2
Pb 4f
Intensity (a.u.)
150 147 144 141 138 135
Binding Energy (eV)
(f)
CsPbBr3
Br 3d5/2
Br 3d3/2
Br 3d
Intensity (a.u.)
72 71 70 69 68 67 66 65
Binding Energy (eV)
(g)
CsPbBr3.03
Br 3d5/2
Br 3d3/2
Br 3d
Intensity (a.u.)
72 71 70 69 68 67 66 65
Binding Energy (eV)

Fig. S4 X-ray photoelectron spectroscopy (XPS) analysis of $CsPbBr_3$ crystals and $CsPbBr_{3.03}$ crystals. (a) Wide-scan XPS of $CsPbBr_3$ crystals and $CsPbBr_{3.03}$ crystals (b) Cs 3d XPS of $CsPbBr_3$ crystals. (c) Cs 3d XPS of $CsPbBr_{3.03}$ crystals. (d) Pb 4f XPS of $CsPbBr_3$ crystals. (e) Pb 4f XPS of $CsPbBr_{3.03}$ crystals. (f) Br 3d XPS of $CsPbBr_3$ crystals. (g) Br 3d XPS of $CsPbBr_{3.03}$ crystals.

Table S2. Binding energies of electrons in undoped $CsPbBr_3$ and $CsPbBr_{3.03}$.

Electron binding energy (eV)	Undoped $CsPbBr_3$	$CsPbBr_{3.03}$
Cs $3d_{3/2}$	738.12	734.99
Cs $3d_{5/2}$	724.19	721.06
Pb $4f_{5/2}$	142.87	142.92
Pb $4f_{7/2}$	138.00	138.06
Br 3d3/2	69.05	69.04
Br 3d5/2	68.01	68.00

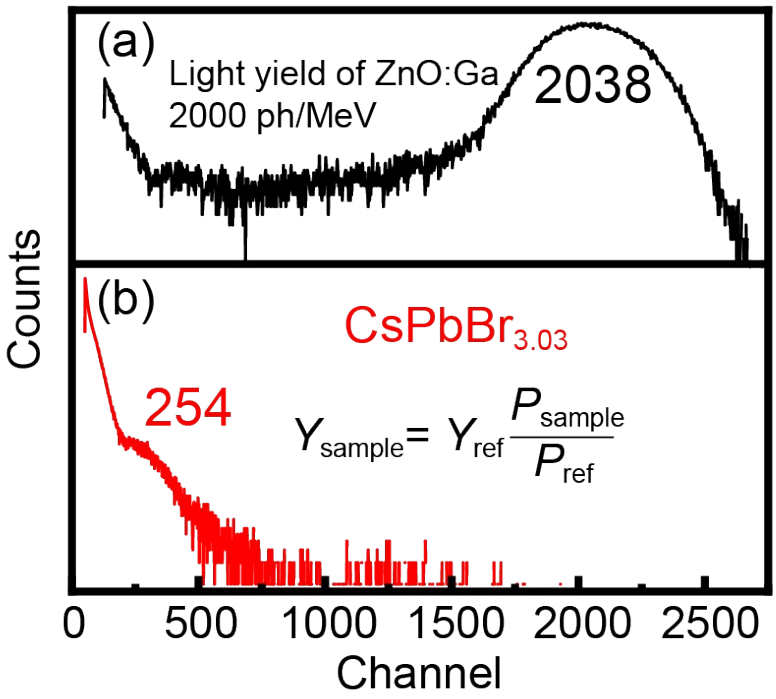

Fig. S5 (a) A comparison of the pulse height spectra obtained when the standard ZnO:Ga sample was excited by the α-particles emitted from ^{241}Am. (b) A comparison of the pulse height spectra obtained when the $CsPbBr_{3.03}$ sample was excited by the α-particles emitted from ^{241}Am.

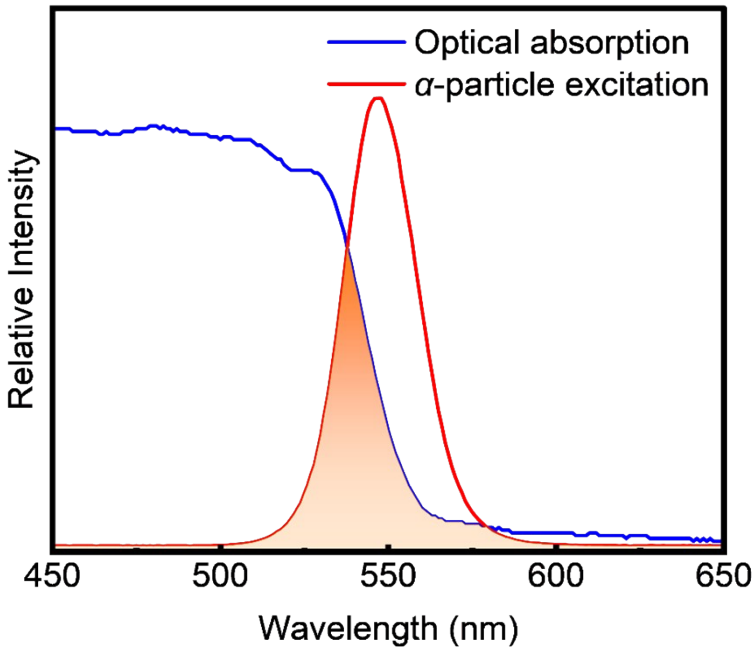

Fig. S6 Stokes shift of $CsPbBr_{3.03}$ crystals.

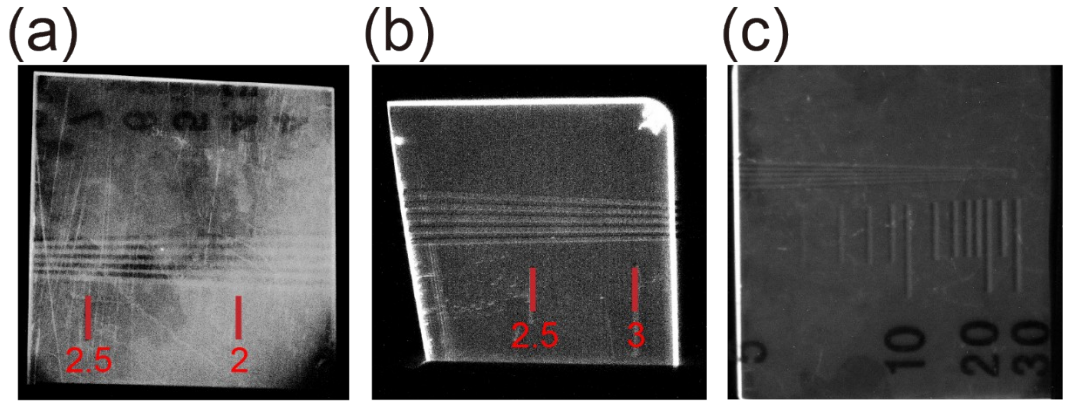

Fig. S7 (a) 1.1-mm-thick $CsPbBr_{3.03}$ single crystal, (b) 1.0-mm-thick $CsPbBr_{3.03}$ single crystal, (c) 0.8-mm-thick $CsPbBr_{3.03}$ single crystal.

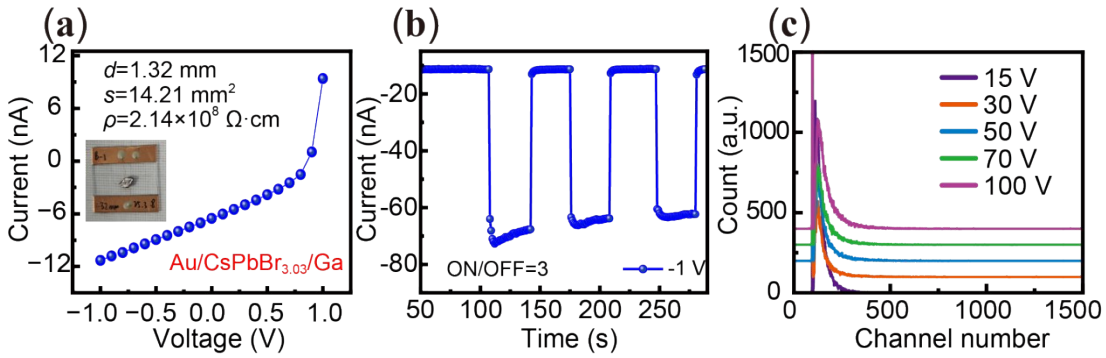

Fig. S8 (a) Current and Voltage (*I-V*) curve of Au/$CsPbBr_{3.03}$/Ga asymmetric electrode structure device, the illustration shows the physical picture of the device. (b) On/off characteristics of Au/$CsPbBr_{3.03}$/Ga device Irradiated by LEDs. (c) Pulsed height energy spectra of Au/$CsPbBr_{3.03}$/Ga device irradiated by 122 keV Gamma-rays from ^{57}Co source under various bias voltage.

Table S3. The calculation results of the volume expansion and formation energy of the undoped and 1% over-doped models. (The supercell employed in the Br-doped model is merely half the size of those utilized in other supercells.)

	volume(Å^3)	Expansion rate/%	Forming energy of Br atom/eV
Pure phase sample	13360	0	0
Doping with a single Br	6685	0.0749	0.301
Doped with Br_2	13408	0.3593	0.164

References

1 H. M. Rietveld, *J. Appl. Crystallogr.*, 1969, **2**, 65-71, DOI:10.1107/S0021889869006558.

2 G. Kresse and J. Furthmüller, *Phys. Rev. B*, 1996, **54**, 11169-11186, DOI:10.1103/PhysRevB.54.11169

3 P. E. Blöchl, *Phys. Rev. B*, 1994, **50**, 17953-17979, DOI: 10.1103/PhysRevB.50.17953.

4 J. P. Perdew, K. Burke and M. Ernzerhof, *Phys. Rev. Lett.*, 1996, **77**, 3865-3868, DOI: 10.1103/PhysRevLett.77.3865.

5 H. J. Monkhorst and J. D. Pack, *Phys. Rev. B*, 1976, **13**, 5188-5192, DOI: 10.1103/PhysRevB.13.5188